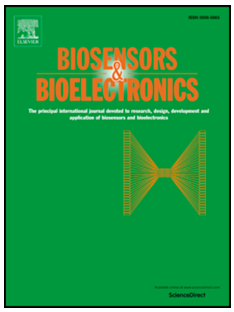

Development of a novel electrochemical immuno-biosensor for circulating biomarkers of the inner ear

Sahar S. Mahshid, Alain Dabdoub

PII: S0956-5663(20)30363-8

DOI: https://doi.org/10.1016/j.bios.2020.112369

Reference: BIOS 112369

To appear in: *Biosensors and Bioelectronics*

Received Date: 5 May 2020

Revised Date: 3 June 2020

Accepted Date: 5 June 2020

Please cite this article as: Mahshid, S.S., Dabdoub, A., Development of a novel electrochemical immuno-biosensor for circulating biomarkers of the inner ear, *Biosensors and Bioelectronics* (2020), doi: https://doi.org/10.1016/j.bios.2020.112369.

Development of a novel electrochemical immuno-biosensor for circulating biomarkers of the inner ear.

Sahar S. Mahshid,[1] Alain Dabdoub, *[1,2,3]

[1] Sunnybrook Research Institute, Toronto, ON M4N 3M5, Canada.

[2] Department of Otolaryngology-Head & Neck Surgery, University of Toronto, Toronto, ON M5S 3H2, Canada.

[3] Department of Laboratory Medicine and Pathobiology, University of Toronto, Toronto, ON M5S 1A1, Canada.

CRediT authorship contribution statement

Sahar Sadat Mahshid: Conceptualization, Methodology, Validation, Formal analysis, Investigation, Resources, Data curation, Writing - Original Draft, and Writing - Review & Editing, Supervision. **Alain Dabdoub:** Conceptualization, Resources, Writing - Review & Editing, and Funding acquisition.

Development of a novel electrochemical immuno-biosensor for circulating biomarkers of the inner ear

Sahar Sadat Mahshid*[1] and Alain Dabdoub *[1,2,3]

[1] Sunnybrook Research Institute, Toronto, ON M4N 3M5, Canada.

[2] Department of Otolaryngology - Head & Neck Surgery, University of Toronto, Toronto, ON M5S 3H2, Canada.

[3] Department of Laboratory Medicine and Pathobiology, University of Toronto, Toronto, ON M5S 1A1, Canada.

S.S.M: https://orcid.org/0000-0002-0834-8787; Email: sahar.mahshid@sri.utoronto.ca

A.D: https://orcid.org/0000-0002-4259-2425; Email: alain.dabdoub@sri.utoronto.ca

* Corresponding authors:

Alain Dabdoub, PhD

Sunnybrook Health Sciences Centre

2075 Bayview Ave., Toronto, ON M4N 3M5, Canada

Phone: 1-416-480-6804

Email: alain.dabdoub@sri.utoronto.ca

Sahar Sadat Mahshid, PhD

Sunnybrook Research Institute

2075 Bayview Ave., Toronto, ON M4N 3M5, Canada

Email: sahar.mahshid@sri.utoronto.ca

Abstract

Current approaches for diagnosis of hearing or vestibular disorders are mostly based on physical examinations that cannot provide information about the exact location of cellular damage inside the inner ear. Therefore, there is a need for new diagnostic methods capable of identifying the sites of damage through the detection of inner ear blood-circulating biomarkers. Here, we developed the first biosensor platform for rapid detection of otolin-1 and prestin, blood-circulating proteins specifically expressed in the vestibule and cochlea, respectively. The platform was designed on a DNA-based immunoassay that employed conjugated antibodies for target protein recognition, which when bound, altered the DNA-DNA hybridization on the surface, resulting in generation of a concentration-dependent signal. The signal was recorded when the redox moiety brought to the surface by the target enabled a selective electrochemical output directly in whole blood. Signal amplification was acquired by employing high-curvature nanostructured electrodes for sensitive sample analysis at picomolar concentrations with a three-fold quantitative range. The combination of nanostructuring and optimum density of the probes on the surface provided low-picomolar detection limits while utilizing small 10 µL sample volume with a 10-minute response time. The proposed immuno-biosensor is highly selective and quantitative and can easily be adapted for rapid detection of any blood-circulating protein using their specific antibodies as recognition elements.

Keywords

Rapid diagnostics, Electrochemical biosensor, Cochlea, Hearing loss, Vestibular disorders, Point-of-care.

1. Introduction

In the past two decades, rapid accurate diagnostic approaches based on the detection of biomarkers have been penetrating in many areas of medical diagnostics including infectious diseases (Laksanasopin et al., 2015; Pang et al., 2019), cancers (Mattox et al., 2019), and neurological disorders (Moon et al., 2018; Wei et al., 2018), but not yet inner ear diseases. In fact, current methods to measure inner ear function utilize a set of physical and neurological examinations such as audiograms (Stapells and Oates, 1997) (for hearing thresholds), vestibular evoked myogenic potentials (Rosengren et al., 2010) (for vestibular function), or posturography (Visser et al., 2008) (for balance evaluations), which do not indicate the specific sites of degeneration within the inner ear (Landegger et al., 2016). Permanent damage to the cellular sites of the inner ear – sensory hair cells, neurons, synapses, or stria vascularis – due to noise exposure, aging, and side effect of antibiotics (aminoglycosides) or chemotherapeutic drugs (cisplatin) can result in hearing loss and/or vestibular disorders (Liberman et al., 2016; Moser and Starr, 2016), which can only be identified post mortem. This leads clinicians to adopt a one-size-fits-all-approach to the treatment, as they are not equipped with the information required to apply targeted treatment or rehabilitation for the specific injury. As new strategies based on gene and stem cell therapies are being developed (Meas et al., 2018; Nacher-Soler et al., 2019; Omichi et al., 2019; Samarajeewa et al. 2019; Taiber and Avraham, 2019), there is an unmet need for the development of novel diagnostic approaches based on the detection of inner ear effective biomarkers circulating in the blood, to be able to identify the sites of cellular damage resulting in more precise diagnostics to ultimately guide therapy.

The lack of knowledge about inner ear specific biomarkers has been a main challenge toward the development of such advancements. However, recent studies have shown the alteration of a number of serum proteins in human and animal models as indicators of inner ear disorders (Avallone et al., 2018;

Doğan et al., 2019; Hana and Bawi, 2018; Naples et al., 2018). Otolin-1 is a scaffolding protein expressed in the utricle and saccule – the otolith organs which are part of the vestibular component of the inner ear (Deans et al., 2010), and prestin is a motor protein uniquely expressed in the cochlea, particularly in outer hair cells (Dallos and Fakler, 2002; Mio et al., 2008). Changes in serum otolin-1 levels are detectable in patients with balance/vestibular end organ problems such as benign paroxysmal positional vertigo (Parham et al., 2014). Furthermore, in an animal-ototoxicity model, changes in prestin blood levels were detectable before any shifts in audiometric thresholds could be traced (Parham and Dyhrfjeld-Johnsen, 2016), indicating the ability of the two proteins to perform as potential biomarkers for inner ear blood-based diagnosis.

Recently, approaches for rapid point-of-care detection of macromolecules, particularly proteins, for disease diagnostics have been developed with the aim of reducing the time and limit of detection compared to currently available multiple-step detection processes (e.g., enzyme-linked immunosorbent assay (ELISA) (Engvall and Perlmann, 1971) and Western blots (Towbin et al., 1979)) (Budhathoki-Uprety et al., 2019; Chinnadayyala et al., 2019; Hassan et al., 2017). Among platforms based on optical or mass detection, the electrochemical biosensors, in principle, provide selectivity for capturing target molecules while delivering a specific measurable signal (Chen et al., 2020; Labib et al., 2016). However, achieving high levels of sensitivity and selectivity in whole blood remains challenging. In this case, various recognition strategies are proposed utilizing antibodies, proteins, synthetic DNAs, and small-molecules interactions with the target of interest (Chambers et al., 2008; Lin et al., 2016; Mahshid et al., 2019; Mahshid et al., 2017a; Ricci et al., 2012). Furthermore, the sensor's surface, when combined with nanostructured electrodes, offers a large surface area in small sample volumes (Mahshid et al., 2016), and enhancement in the molecular capturing mechanism on the limited geometry of the

surface (De Luna et al., 2017), resulting in the improvement of the sensitivity and detection limit of electrochemical biosensors (Kelley et al., 2014).

Here, we developed the first biosensor platform utilizing a DNA-based immunoassay immobilized on nanostructured electrodes for the detection of otolin-1 and prestin proteins, which are potential biomarkers of balance and hearing disorders, respectively. Taking advantage of the steric hindrance mechanism (Mahshid et al., 2015) on the nanostructured electrodes (Mahshid et al., 2017b), we designed a recognition strategy adapting the conjugated antibodies that can be extended further to a variety of different target proteins by incorporating their specific antibodies. The proposed electrochemical biosensor can potentially overcome the challenges toward one-step rapid detection at the point-of-care.

2. Materials and Methods

Reagents. Glass chips (Telic; Valenica, CA), $HAuCl_4$ solution (Sigma-Aldrich), 6N-hydrochloric acid (HCl; VWR), Tris(2-carboxyethyl) phosphine hydrochloride (TCEP; Sigma-Aldrich), 6-Mercapto-1-hexanol (MCH; Sigma-Aldrich), Phosphate-buffered saline (PBS, pH 7.4, 1X; Invitrogen), magnesium chloride ($MgCl_2$; ≥98%; Sigma-Aldrich). The DNA constructs (Table S1) synthesized and HPLC (high-performance liquid chromatography) purified (Biosearch Technologies Inc., Novato, CA), were aliquoted and stored at -20 °C. Biotin-conjugated rabbit polyclonal antibody to human otolin-1 and to human SLC26A5 (prestin) (anti-OTOL1 and anti-PRES; LifeSpan Biosciences Inc.); streptavidin (Sigma-Aldrich), otolin-1 protein antigen (26 kDa; Novus Biologicals) were all aliquoted and stored at -20°C for long-term storage and at 4°C for short-term use. SLC26A5 or prestin protein (81.4 kDa; Novus Biologicals) was aliquoted and stored at -80°C. Single-donor human whole blood from Innovative Research, that contains heparin as an anticoagulant, was aliquoted and frozen at -20°C prior to use.

Instrumentation. Chronoamperometry and square wave voltammetry (SWV) was carried out by PalmSens4 potentiostat/galvanostat/impedance analyzer combined with MUS08R2 multiplexer (PalmSens Instruments, Netherland). A conventional three-electrode cell was used with a platinum wire counter electrode (CE; Sigma-Aldrich), an Ag/AgCl reference electrode (RE; CH Instruments), and the chip substrate as the working electrode.

On-chip electrode preparation. Glass chips were patterned with the leads and the electrodes at their terminals by first precoating with a 5 nm-Cr, coating with a 50 nm-Au, coating with a layer of AZ 1600 positive photoresist, selective exposure to 900 W UV for 12 s, developing in MF 312 for 40 s, and wet etching of Au and Cr on the unprotected areas. The 10 µm-apertures were then formed on the electrodes by spin-cast of the negative photoresist (SU-8 2002) at 4500 rpm for 40 s on the patterned chips, exposing for 12 s, and then developing for 1 min. Chip substrates with twenty addressable 10 µm-apertures were rinsed with acetone, isopropyl alcohol, and deionized water (DI water), then dried with the flow of nitrogen (Figure S1, steps 1 to 7).

Chips were immersed in a 3 ml electrolyte solution containing 50 mM $HAuCl_4$ and 0.5 M HCl. The gold nanostructured electrodes (NEs) were electrodeposited on the apertures using chronoamperometry at 0 mV for 200 s (for 200 µm NE1 and NE2) and 100 s (for 100 µm NE3). All the experiments were done at room temperature. The chips were then rinsed with DI water and dried by air-blowing to become ready for capturing probe immobilization (Figure S1, step 8).

Surface immobilization was done with 100 nM and 200 nM capturing probes in 1X PBS + 10 mM $MgCl_2$. Prior to immobilization, 1 µl of 0.1 mM capturing probes were incubated with 2 µl of 10 mM TCEP for 1 hr for reduction of disulfide bonds, then diluted in 1X PBS + 10 mM $MgCl_2$ to the desired concentrations; 100 µL of capturing probe solutions of 100 nM (on NE1 and NE3) and 200 nM (on NE2) were applied on the individual chips, to cover all the area of the electrodes and kept overnight.

After washing with 1X PBS, 100 µL of 3 mM MCH was put on the electrodes for 3 hr and then washed with 1X PBS. The surface density of the capturing probes was calculated between 1×10^{12} – 5×10^{12} cm^{-2} depending on the size of the electrode (Figure S1, steps 9 and 10) (Mahshid et al., 2015). Scanning electron microscopy (SEM) images of the electrodes' microstructure were acquired before immobilization using a Quanta FEG 250 ESEM (Figure S1). The electrodes were stable after several days of storage at 4°C as demonstrated by testing (Figure S2).

Electrochemical measurement. SWV was used to collect the experimental data from -0.45 to 0.05 V in increments of 0.001 V *vs*. Ag/AgCl, with an amplitude of 50 mV and a frequency of 60 Hz. Peak currents were fitted using the PSTrace software (PalmSens Instruments).

In buffer media: The recognition complex was prepared by pre-incubation of antibodies with streptavidin (1:1) overnight. Then the signaling probe was added to the mixture (5:1) and (10:1) overnight to make a final recognition solution of 25 nM signaling probe + 5 nM streptavidin-conjugated-antibody and 10 nM signaling probe + 100 pM streptavidin-conjugated-antibody, respectively.

In human whole blood (≥71%): 10 µL of the pre-(overnight)incubated recognition complex solution of 20 nM (described above) is mixed with 1 µL of the 1 µM signaling probe overnight and reached to 40 µL volume by adding whole blood. Proteins were first spiked in whole blood (0.2 µL of protein to 10 µL of whole blood) prior to mixing with the recognition compound.

All measurements were taken immediately after 15 min incubation of protein with the mixture of recognition bound to signaling probe solution. For the incubation, the chips were divided into two zones using a hydrophobic pen (showed Figure 1), each having ten electrodes that were loaded with 10 µL-solution. One of the zones on the chip was always assigned for the control test. After 10 min of acquisition (will later be extracted from Figure 3), the chips were unloaded and reloaded with 1X PBS or

with whole blood (100%) for the signal measurement in buffer media and whole blood, respectively. Results are presented in terms of current (knowing that the geometric area of the electrode is 0.03 mm^2 for NE1 and NE2 and 0.008 mm^2 for NE3). Control samples (ctrl.) represent the response to 10 nM of signaling probes after 10 min.

Gain reduction. This value was calculated as the difference in peak current of the samples with and without the target protein divided by the initial peak current (without target protein).

Binding curve. Binding curves or dose-response curves were obtained by testing various concentrations of protein on the platform. Individual curves were fitted to a single-site binding mechanism. C0 = background current; C50% is the concentration of target proteins when the sensor reaches 50% of the signal amplitude:

$$C_{[Target]} = C_0 + \left(\frac{[Target](current\ amplitude)}{[Target] + C_{50\%}}\right)$$

Probe density calculations. Capturing probe surface density is defined by the number of moles of capturing probes per unit area of the NE (N_t) that is equivalent to the number of redox moiety, methylene blue (MB) being placed on the surface through hybridization: n = 2, number of electrons transferred per MB label; F, Faraday constant; R, universal gas constant; T, temperature; Eac, amplitude; f, frequency of the applied voltage perturbation.

$$peak\ current = 2nfFN_t \frac{sinh\left(\frac{nFEac}{RT}\right)}{cosh\left(\frac{nFEac}{RT}\right) + 1}$$

We estimated the capturing probes surface density on three different NEs (based on the size and immobilization concentration) after 10 min of hybridizing to 100 nM signaling probes (Table 1).

Table 1. The estimated density of capturing probes.

	area, cm^2	*[probe], nM*	*density, $1/cm^2$*
NE1	***0.0003***	***100***	$\boldsymbol{(1.26\pm 0.38)\times 10^{12}}$
NE2	***0.0003***	***200***	$\boldsymbol{(4.57\pm 0.84)\times 10^{12}}$
NE3	***0.00008***	***100***	$\boldsymbol{(3.64\pm 0.56)\times 10^{12}}$

Statistics. Data for bar charts and binding curves are reported as mean values ± standard errors of the means and were analyzed using GraphPad Prism 8.0 (GraphPad Software Inc., San Diego, CA). Data for Figures 1C-blue, 2, and 4 were analyzed by one-way analysis of variance (ANOVA) with omnibus statistics in Table S2. *Post hoc* comparisons were done by Tukey's Honest Significant Difference (HSD) test. P-values below the alpha criterion (probability of Type 1 error) of 0.05 were considered statistically significant in all *post hoc* tests, whereas the alpha criterion for one-way ANOVA tests (described in Table S2) were Bonferroni-corrected due to multiple testing. For the data in Figure 1C-green, the independent *t*-tests were done for the analysis with statistics in Table S3.

3. Results

Overview of approach. We designed a single-step assay taking advantage of the specificity of interactions of oligonucleotide sequences in the sensor's signal, even when deployed in complex media (Drummond et al., 2003) (Figure 1). We electrodeposited nanostructures with high curvature, as working electrodes (NEs) on the 10 µm-apertures of a glass chip with twenty addressable leads (Figure 1A). The nanostructuring of the surface provides tunable sensitivities and linear detection ranges for the electrochemical detection platform. Short single-strand capturing DNA probes (blue strands) are immobilized on the gold nanostructures (Figure 1B). The signaling DNA probes (orange strands) are shorter and complementary to the capturing strands, which upon hybridization, can bring the redox

moiety (here, the MB), to the surface and generate a current signal (Figure 1B', top row). On the other extremity, the signaling probes carry the recognition element utilizing a streptavidin-biotin interaction. This can apply steric effects on surface hybridization, which can be diminished within the curvatures of the nanostructured surface. When the target protein is bound to the recognition element on the signaling DNA probe (Figure 1B'', bottom row), steric hindrance is increased, limiting the number of successful hybridizations to the surface resulting in a reduction in the current signal (blue curve vs. black curve).

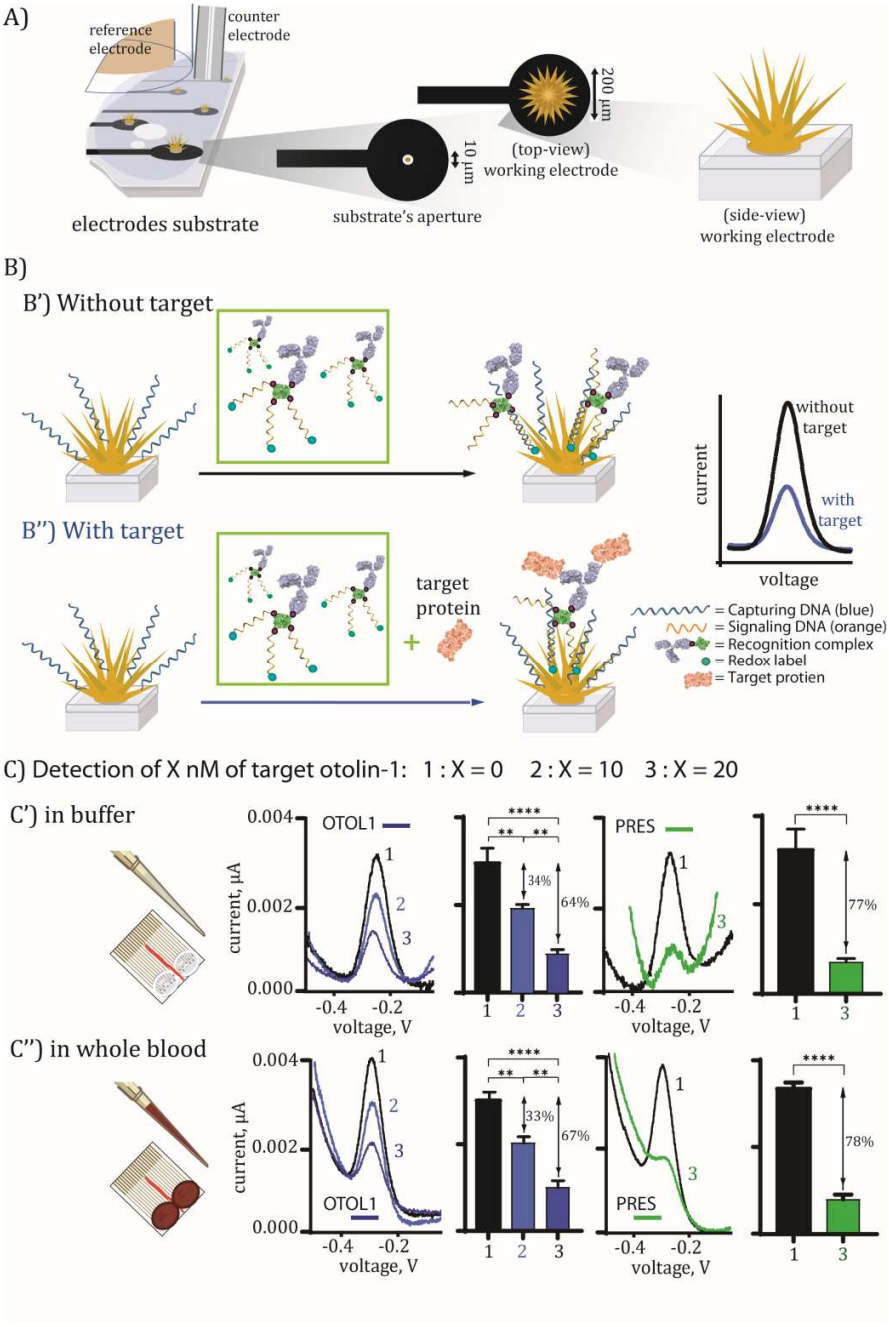

Figure 1. Schematic illustration and proof of principle for the immunosensor developed on nanostructures. (**A**) The 20-lead chip having 200 µm nanostructures electrodeposited (top) on the 10 µm-apertures (bottom) of addressable electrodes. (**B**) The immunoassay has a layer of capturing probes immobilized on the surface of nanostructures. When not attached to the target proteins (**B'**, top), the current signal from hybridization of signaling probes carrying the recognition-antibodies is relatively

high (black). Upon binding to the target protein (B'', bottom), the steric hindrance of target proteins will reduce the number of successful hybridizations to the surface and consequently suppress the current signal (blue). (**C**) The sensor's performance was tested and confirmed to be similar in PBS buffer (**C'**) and in whole blood (C'') by comparing the signal gain reduction at 10 nM (34% vs 33%) and 20 nM (64% vs 67%) of otolin-1 (OTOL1-blue) and 20 nM (77% vs 78%) of prestin (PRES-green). Sample media: 1X PBS+10 mM $MgCl_2$ buffer, and 100% human whole blood; recognition compound: 5 nM of streptavidin-conjugated antibody previously bound to 25 nM of signaling probes; chips were divided into two zones with a hydrophobic line, each zone was loaded with 10 µL of target solution for 10 min-incubation, and kept in a humid chamber; ****P < 0.0001, **P < 0.01.

Detection of otolin-1 and prestin. The mammalian inner ear contains proteins that circulate in the bloodstream. Otolin-1, a glycoprotein expressed within the vestibular supporting cells, provides a scaffold for otoconia on the sensory epithelia maintaining the body balance (Parham et al., 2014). Prestin is a motor protein in the cellular membrane of outer hair cells and operates to elongate the cells in support of normal hearing sensitivity (Liberman et al., 2002). As proof of principle to our DNA-based immunoassay, we targeted protein detection (here, a 26-kDa otolin-1 antigen and an 81-kDa prestin) in buffer as well as in whole blood (Figure 1C). To do so, we first designed a recognition element by having their antibodies (anti-otolin-1 and anti-prestin) attached to the signaling probes via streptavidin-biotin conjugation. Then the sensor platform was developed to maintain the steric hindrance of the target protein despite the potential steric effects of other components of the assay (e.g. the antibody, streptavidin, or the DNA probes). The incorporation of synthetic DNA probes, combined with the anti-protein specific antibody, regulates the capturing and detection of protein without any interference from the non-specific interactions when deployed in whole blood. This is evident by comparing the signal gain reductions of otolin-1 (OTOL1, blue) in the buffer (34% and 64%) and whole blood (33% and

67%) at 10 nM and 20 nM protein concentrations. The detection of prestin (PRES, green) at 20 nM, further proved the similarity of the sensor's response in the buffer (77%) and whole blood (78%). The increase in the signal gain of prestin compared to otolin-1 (78% vs. 67%) could be attributed to the difference in the size of the target proteins (26 kDa vs. 81 kDa). Furthermore, increasing the concentration of protein (10 nM to 20 nM) resulted in more signal loss (33% vs. 67%), representing the quantitative ability of the sensor even in whole blood.

Immunoassay design and validation for otolin-1 and prestin. Surface immobilization was done on nanostructures via sulfur-gold bonds, at a high surface density of the capturing probes, followed by back-filling with the MCH. We used a thiol-modified (on the 5' end) 32-base DNA construct, as the capturing probe on the electrode's surface. The current response of such a surface represents no peak (Figure 2- (1, 1', and 1")). Signaling probes were designed to be 16-base long with a biotin on the 5' end and the MB on the 3' end, complementary to the lower half of the capturing probe construct. Upon hybridization to the high-density of capturing probes on the NEs, a relatively high peak current was measured as the MB is placed on the electrode surface resulting in a successful electron transfer (Figure 2- (2, 2', and 2")). The response peak was not affected by the presence of otolin-1 (OTOL1-blue) and prestin (PRES-green) proteins (3, 3'and 3") or their antibodies (4, 4', and 4").

However, once the signaling probes were introduced to the streptavidin (SA, 55 kDa) (Figure 2- (5, 5', and 5'')), or the streptavidin-conjugated antibodies (SA-antiOTOL1 or SA-antiPRES, 210 kDa) (Figure 2- (6, 6', and 6'')), the current signal decreased by 25% and ~60% (SA-anti-OTOL1, 62% and SA-anti-PRES, 58%), respectively. This is due to the interactions between streptavidin and biotin on the signaling probes, and consequently, the steric hindrance of attached molecules on the surface hybridization. A further signal decrease occurred when the recognition molecule was attached to the

target proteins (otolin-1 antigen: 26kDa and prestin: 81kDa), resulting in elevated steric hindrance effect of a bigger molecular compound (OTOL1 compound, 262 kDa and PRES compound, 372 kDa) on the surface hybridization (Figures 2- (7, 7', and 7'').

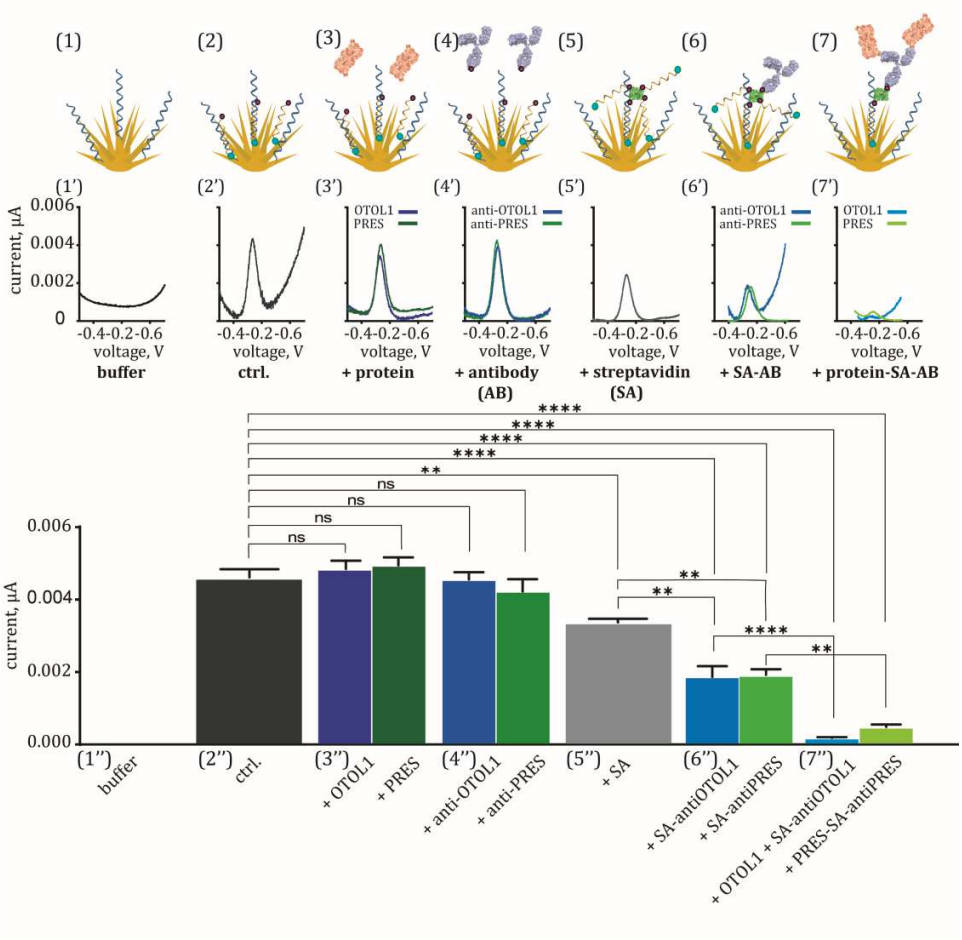

Figure 2. Steric-based assay validation for the detection of otolin-1 and prestin. Assay illustration, square wave voltammetry responses, and the resulting current signal of the immobilized nanostructured electrodes reported, (**1, 1', 1"**) in buffer, then in signaling probes (**2, 2', 2"**) alone, (**3, 3', 3"**) with otolin-1 (OTOL1, blue) or prestin (PRES, green), (**4, 4', 4"**) with otolin-1 antibody (anti-OTOL1, blue) or prestin antibody (anti-PRES, green), (**5, 5', 5"**) with streptavidin (SA), and signaling probes with recognition elements of SA-antiOTOL1 (blue) and SA-antiPRES (green) (**6, 6', 6"**) in the absence of

target, and (**7, 7', 7"**) in the presence of target. ctrl.: control/signaling probes; 10 nM signaling probes, 100 pM recognition element (1:1 SA:antibody), 500 pM otolin-1 and 500 pM prestin protein; buffer media: PBS 1X 10 mM $MgCl_2$. ****P < 0.0001, ***P < 0.001, *P < 0.05, and ns: non-significant.

The signal suppression within this assay originated from, first, the smaller number of signaling probes reaching the surface due to the steric hindrance of attached macromolecules, and second, their lower rate of hybridization (Mahshid et al., 2017b). We studied the hybridization kinetics of signaling probes carrying the recognition element in the absence and presence of the target otolin-1 (Figure 3A). The calculated rate and time of hybridization (Table 2) indicated that there was a slight delay in hybridization to the surface in the presence of the target. We then measured the increase in the signal gain reduction of the sensor versus time, which shows a gradual decrease after the first few minutes. This implies that the maximum performance of the assay can be achieved within the first 10 min (Figure 3B).

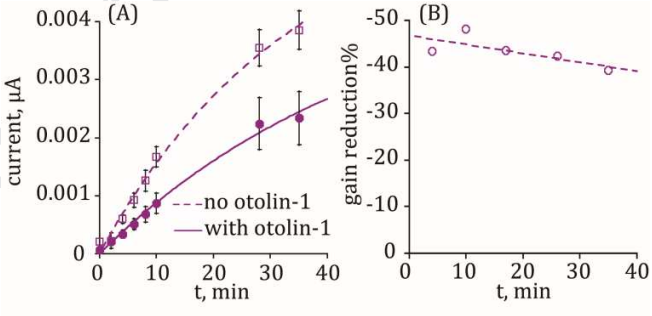

Figure 3. Assay response-time using kinetics and gain reduction. (**A**) Hybridization kinetics of the signaling probes in the absence and presence of target otolin-1. (**B**) The slight changes in the gain reduction versus time, indicating the maximum performance of the assay was within the first 10 min.

284 **Table 2. The hybridization kinetics and the consequent rate and time of hybridization.**

	k, min^{-1}	$t_{1/2}$, min
no target	***0.03***	***23***
with target	***0.02***	***37***

287

288 *Immunoassay optimization.* The maximum surface density of capturing probes combined with the
289 optimum size of the electrode is required to differentiate the signal of the target protein from the
290 background signal (steric hindrance of the conjugated antibody with and without target protein). Then,
291 the minimum amount of signaling probes required to saturate the surface hybridization, and the
292 minimum amount required to generate a measurable signal, can be deducted from the dose-response
293 curves on three NEs with variations in size and immobilized-capturing probe concentration – NE1 (200
294 µm, 100 nM), NE2 (200 µm, 200 nM) and NE3 (100 µm,100 nM) (Figure 4 A, A'). We used tree-like
295 nanostructures that possess high-curvatures to ensure high-surface density of capturing probes as well
296 as high density of hybridization to the surface (De Luna et al., 2017). In this case, we showed that when
297 the immobilization concentration is adjusted to 100 nM, and the concentration of the signaling probe to
298 10 nM, we could maintain a high current signal as well as minimize the background current induced by
299 the large (210 kDa) recognition element.

300 We also estimated the minimum amount of recognition molecule required to maintain the steric
301 hindrance of the target molecule once it was attached to the signaling probe, as well as a high current
302 signal in the absence of the target molecule. The dose-response curves of the recognition molecules were
303 measured with 10 nM of signaling probes (deducted from $C_{50\%}$ of Figure 4 A, A') on the NEs (Figure 4
304 B, B'; $C_{50\%,NE1}$ = 750 pM and $C_{50\%,NE3}$ = 85 pM) implying that the smaller NEs (NE3) were capable of

complete suppression of the background current. With an optimum amount of recognition element (data is shown for 100 pM), we then conducted the binding curve of target protein (here, otolin-1; Figure 4 C, C'). The resulting $C_{50\%}$ was measured at 280 pM on NE1 and 2 pM on NE3. We showed that with NE3, we could detect low picomolar concentrations of the protein within a three-fold quantitative range within less than 10 min, which demonstrated the capacity of this technique for rapid point-of-care detection of proteins.

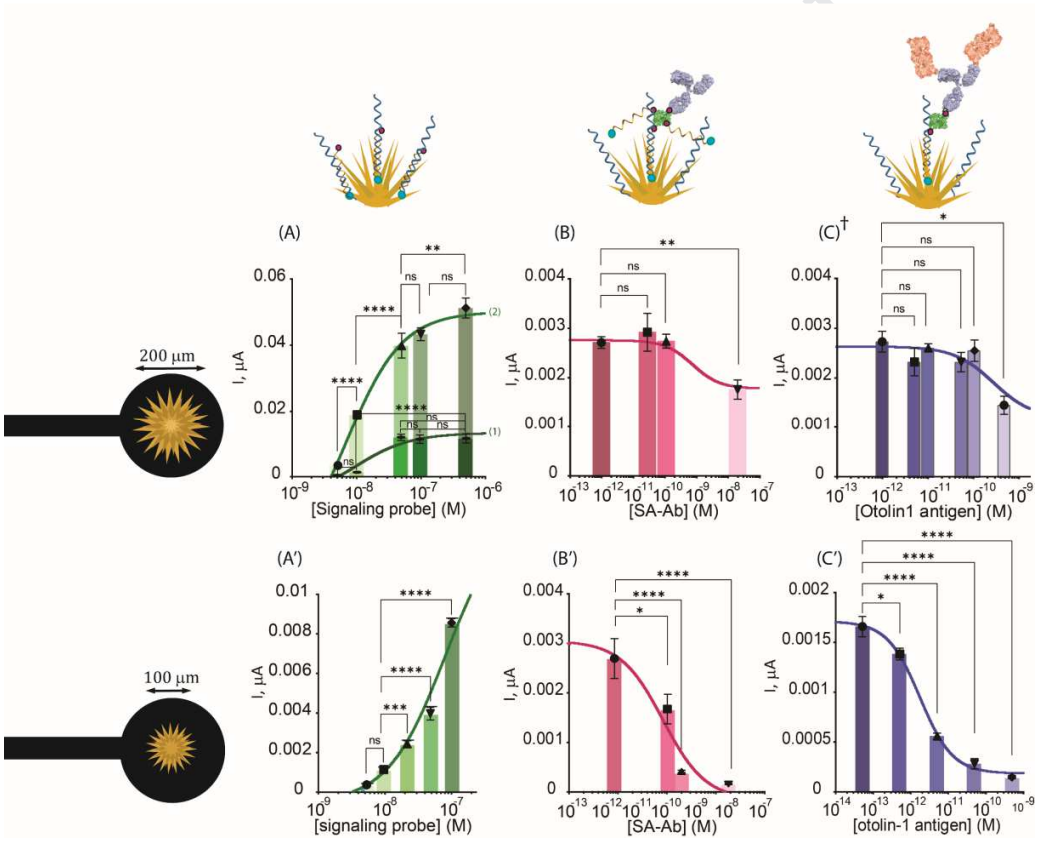

Figure 4. Optimization of the assay through the study of dose-response curves. Comparison of dose-response curves on NE1, NE2, NE3 when applied in signaling probes (**A, A'**) without recognition element have C50%, A, NE1 = 16±3 nM; C50%, A, NE2 = 10±3 nM; and C50%, A', NE3 = 85±13 nM; and (**B, B'**) with recognition element in the absence of protein have C50%, B, NE1 = 750 nM and C50%, B', NE3 = 85 nM; and (**C, C'**) with recognition element in the presence of protein have C50%,

C, NE1 = 280 pM and C50%, C', NE3 = 2 pM. NEs 1 to 3 are introduced in Table 1; ****P < 0.0001, ***P < 0.001, *P < 0.05, and ns: non-significant. †Although the ANOVA model for panel 4C was not significant, at the highest level of the Otolin1 antigen (500 pM), the reduction in the response was at the start of the dose-response curve and had significantly reduced (*P<0.05).

4. Discussion

Using the idea of steric hindrance on nanostructured surfaces that could alter the hybridization of DNA probes to their complementary strands on the surface generating a measurable linear range, we created the first biosensor for electrochemical detection of otolin-1 and prestin, two circulating biomarkers of the mammalian inner ear. Compared with the complicated multiple-step ELISA-based approaches that are used as the gold standard for the detection of inner ear proteins, our approach has the advantage of rapidity and specificity of the signal, making it a strong candidate for the point-of-care diagnostic platforms for inner ear diseases. Although this report is on the detection of two inner ear proteins, otolin-1 and prestin, it can be adapted for other inner ear biomarkers as well as for any other circulating protein biomarkers.

Our DNA-based detection platform incorporates a recognition strategy with an antibody conjugated to streptavidin for the detection of proteins at low concentrations. In this case, a combination of the high density of capturing DNA probes on the surface, and an optimal density of signaling complementary DNA probes carrying the streptavidin-antibody recognition element to the surface was calculated to ensure the best performance of the assay on the nanostructured electrodes for quantitative detection of protein. We showed that by using small-scale nanostructured electrodes, we could improve the sensitivity down to low picomolar concentrations with a three-fold linear detection range. We also demonstrated the assay detection time is less than ten minutes, indicating that the assay can be utilized for rapid diagnostic techniques.

The physiological levels of otolin-1 and prestin in human blood are in the femtomolar ranges. Their variations start from around 1 fM (~100 pg/ml) in healthy individuals to about 15 fM (~1000 pg/ml) depending on the age and level of damage (Doğan et al., 2019; Parham et al., 2014; Tabtabai et al., 2017). While quantitative measurements within whole blood can be challenging, mainly when detecting low physiological levels, such as for the inner ear proteins (Kelley et al., 2014; Yousefi et al., 2019), we proposed a strategy to reduce the detection limit and yet maintain the linearity of the sensor by lowering the electrode's dimension while enabling the high curvatures of nanostructuring. The combination of synthetic assays with nanostructured electrodes can also be improved to promote the rate of reactions and can be adapted within a microfluidic device to accelerate the rate of target delivery and develop a rapid test platform in therapeutic ranges.

5. Conclusion

Better diagnostics are needed to distinguish the cellular site of lesion in hearing and balance organs. Here, we developed an electrochemical immuno-biosensor that can detect two inner ear biomarkers in whole blood. We have shown that we are able to detect these proteins rapidly and at low concentrations providing potential opportunities for use at the point-of-care. In the future, in order to ameliorate hearing and balance disorders, we need to identify new diagnostic and prognostic biomarkers to better understand disease initiation and progression and be able to assess treatment efficacy. Our biosensor platform can be utilized for newly discovered inner ear protein biomarkers as well as other disease biomarkers.

Declaration of competing interests

The authors declare no competing interests.

CRediT authorship contribution statement

Sahar Sadat Mahshid: Conceptualization, Methodology, Validation, Formal analysis, Investigation, Resources, Data curation, Writing - Original Draft, and Writing - Review & Editing, Supervision. **Alain Dabdoub:** Conceptualization, Resources, Writing - Review & Editing, and Funding acquisition.

Acknowledgments

We thank Drs. E. Luca, A.M. Higazi, and D. Rocco for helpful discussions and assistance on the molecular validation techniques. We also thank Dr. B.T. Paul for helpful discussions on the statistical analysis and Dr. S. Cushing for commenting on the manuscript. This work was supported by a grant from the Krembil Foundation (AD) and by the Koerner Foundation.

Appendix A: Supplementary material

Supplementary data to this article can be found online and includes: Figure 1S. Preparation process of the nanostructured electrodes and their SEM microstructure. Figure 2S. Testing the electrodes stability after several days of storage. Table S1. Sequences of capturing and signaling DNA probes; Table S2. Statistics measured by one-way analysis of variance for otolin-1 and prestin electrochemical immuno-biosensor; Table S3. Statistics measured by independent t-tests for prestin electrochemical immuno-biosensor.

References

Avallone, E., Schmitt, H., Lilli, G., Warnecke, A., Lesinski-Schiedat, A., Lenarz, T., Willenborg, K., 2018. Laryngo-Rhino-Otologie 97(S 02), 10428-1.

Budhathoki-Uprety, J., Shah, J., Korsen, J.A., Wayne, A.E., Galassi, T.V., Cohen, J.R., Harvey, J.D., Jena, P.V., Ramanathan, L.V., Jaimes, E.A., Heller, D.A., 2019. Nat. Commun. 10, 3605-9.

Chambers, J.P., Arulanandam, B.P., Matta, L.L., Weis, A., Valdes, J.J., 2008. Curr. Issues Mol. Biol. 10, 1-12.

Chen, L.-C., Wang, E., Tai, C.-S., Chiu, Y.-C., Li, C.-W., Lin, Y.-R., Lee, T.-H., Huang, C.-W., Chen, J.-C., Chen, W.L., 2020. Biosens. Bioelectron. 155, 112111-8.

Chinnadayyala, S.R., Park, J., Le, H.T.N., Santhosh, M., Kadam, A.N., Cho, S., 2019. Biosens. Bioelectron. 126, 68-81.

Dallos, P., Fakler, B., 2002. Nat. Rev. Mol. Cell Biol. 3, 104-111.
De Luna, P., Mahshid, S.S., Das, J., Luan, B., Sargent, E.H., Kelley, S.O., Zhou, R., 2017. Nano Lett. 17, 1289-1295.
Deans, M.R., Peterson, J.M., Wong, G.W., 2010. PloS one. 5, e12765-15.
Doğan, M., Şahin, M., Kurtulmuş, Y., 2019. J. Int. Adv. Otol. 15, 200-203.
Drummond, T.G., Hill, M.G., Barton, J.K., 2003. Nat. Biotechnol. 21, 1192-1199.
Engvall, E., Perlmann, P., 1971. Immunochemistry 8, 871-874.
Hana, R.S., Bawi, B.L., 2018. Ibnosina J. Med. Biomed. Sci. 10, 60-64.
Hassan, U., Ghonge, T., Reddy Jr, B., Patel, M., Rappleye, M., Taneja, I., Tanna, A., Healey, R., Manusry, N., Price, Z., Jensen, T., Berger, J., Hasnain, A., Flaugher, E., Liu, S., Davis, B., Kumar, J., White, K., Bashir, R., 2017. Nat. Commun. 8, 15949-12.
Kelley, S.O., Mirkin, C.A., Walt, D.R., Ismagilov, R.F., Toner, M., Sargent, E.H., 2014. Nat. Nanotechnol. 9, 969-980.
Labib, M., Sargent, E.H., Kelley, S.O., 2016. Chem. Rev. 116, 9001-9090.
Laksanasopin, T., Guo, T.W., Nayak, S., Sridhara, A.A., Xie, S., Olowookere, O.O., Cadinu, P., Meng, F., Chee, N.H., Kim, J., 2015. Sci. Transl. Med. 7, 273re271-273re271.
Landegger, L.D., Psaltis, D., Stankovic, K.M., 2016. Hear. Res. 335, 83-93.
Liberman, M.C., Epstein, M.J., Cleveland, S.S., Wang, H., Maison, S.F., 2016. PloS One. 11, e0162726-15.
Liberman, M.C., Gao, J., He, D.Z., Wu, X., Jia, S., Zuo, J., 2002. Nature 419, 300-304.
Lin, M., Song, P., Zhou, G., Zuo, X., Aldalbahi, A., Lou, X., Shi, J., Fan, C., 2016. Nat. Protoc. 11, 1244-1263.
Mahshid, S., Mepham, A.H., Mahshid, S.S., Burgess, I.B., Saberi Safaei, T., Sargent, E.H., Kelley, S.O., 2016. J. Phys. Chem. C 120, 21123-21132.
Mahshid, S.S., Camire, S., Ricci, F., Vallee-Belisle, A., 2015. J. Am. Chem. Soc. 137, 15596-15599.
Mahshid, S.S., Mahshid, S., Vallée-Bélisle, A., Kelley, S.O., 2019. Anal. Chem. 91, 4943-4947.
Mahshid, S.S., Ricci, F., Kelley, S.O., Vallée-Bélisle, A., 2017a. ACS Sens. 2, 718-723.
Mahshid, S.S., Vallée-Bélisle, A., Kelley, S.O., 2017b. Anal. Chem. 89, 9751-9757.
Mattox, A.K., Bettegowda, C., Zhou, S., Papadopoulos, N., Kinzler, K.W., Vogelstein, B., 2019. Sci. Transl. Med. 11, eaay1984-4.
Meas, S.J., Zhang, C.-L., Dabdoub, A., 2018. Front. Mol. Neurosci. 11, 77-12.
Mio, K., Kubo, Y., Ogura, T., Yamamoto, T., Arisaka, F., Sato, C., 2008. J. Biol. Chem. 283, 1137-1145.
Moon, J.-M., Thapliyal, N., Hussain, K.K., Goyal, R.N., Shim, Y.-B., 2018. Biosens. Bioelectron. 102, 540-552.
Moser, T., Starr, A., 2016. Nat. Rev. Neurol. 12, 135-149.
Nacher-Soler, G., Garrido, J.M., Rodríguez-Serrano, F., 2019. Arch. Med. Sci. 15, 957-967.
Naples, J., Cox, R., Bonaiuto, G., Parham, K., 2018. Otolaryngology–Head and Neck Surgery 158, 541-546.
Omichi, R., Shibata, S.B., Morton, C.C., Smith, R.J., 2019. Hum. Mol. Genet. 28, R65-R79.
Pang, Y., Wang, C., Lu, L., Wang, C., Sun, Z., Xiao, R., 2019. Biosens. Bioelectron. 130, 204-213.
Parham, K., Dyhrfjeld-Johnsen, J., 2016. Otol Neurotol. 37, 1217-1222.
Parham, K., Sacks, D., Bixby, C., Fall, P., 2014. Otolaryngology–Head and Neck Surgery 151, 1038-1040.
Ricci, F., Adornetto, G., Palleschi, G., 2012. Electrochim. Acta 84, 74-83.
Rosengren, S., Welgampola, M., Colebatch, J., 2010. Clin. Neurophysiol. 121, 636-651.

Samarajeewa, A., Jacques, B.E., Dabdoub, A., 2019. Mol. Ther. 27, 904-911.
Stapells, D.R., Oates, P., 1997. Audiol. Neurotol. 2, 257-280.
Tabtabai, R., Haynes, L., Kuchel, G.A., Parham, K., 2017. Otol Neurotol. 38(6), 865-869.
Taiber, S., Avraham, K.B., 2019. Neurosci. Lett. 713, 134527-9.
Towbin, H., Staehelin, T., Gordon, J., 1979. Proc. Natl. Acad. Sci. 76, 4350-4354.
Visser, J.E., Carpenter, M.G., van der Kooij, H., Bloem, B.R., 2008. Clin. Neurophysiol. 119, 2424-2436.
Wei, T.-Y., Fu, Y., Chang, K.-H., Lin, K.-J., Lu, Y.-J., Cheng, C.-M., 2018. Trends Biotechnol. 36, 290-303.
Yousefi, M., Dehghani, S., Nosrati, R., Zare, H., Evazalipour, M., Mosafer, J., Tehrani, B.S., Pasdar, A., Mokhtarzadeh, A., Ramezani, M., 2019. Biosens. Bioelectron. 130, 1-19.

Development of a novel electrochemical immuno-biosensor for circulating biomarkers of the inner ear.

Sahar Sadat Mahshid *[1] and Alain Dabdoub *[1,2,3]

[1] Sunnybrook Research Institute, Toronto, ON M4N 3M5, Canada.
[2] Department of Otolaryngology-Head & Neck Surgery, University of Toronto, Toronto, ON M5S 3H2, Canada.
[3] Department of Laboratory Medicine and Pathobiology, University of Toronto, Toronto, ON M5S 1A1, Canada.

Highlights

- There is no diagnostic test to identify the exact location of inner ear cellular damage.
- A new diagnostic method developed for detecting inner ear circulating biomarkers.
- The immuno-biosensor showed rapid sensitive response to prestin and otolin-1.
- The specificity and robustness of the biosensor was tested in whole blood samples.

Declaration of interests

☒ The authors declare that they have no known competing financial interests or personal relationships that could have appeared to influence the work reported in this paper.

☐The authors declare the following financial interests/personal relationships which may be considered as potential competing interests: